ultra-small optical circuits based on the 3D photonic crystal. Figure 3 shows the first successful fabrication of 3D sharp bend (90°) waveguide, which has been developed here. Two stripe layers, one of which is removed to form a straight air waveguide, are stacked with a crossed configuration to form a 90° bend waveguide, and they are sandwiched by the upper and lower complete photonic crystals. The waveguide is composed of 12 stacked layers in total with a stripe period of 4 μm. The waveguide has a potentially very high transmission (>95%) property in a very wide frequency range from 0.553 to 0.605 [c/a], which was predicted by the finite-difference time-domain calculation (*15*).


**References**

1. E. Yablonovitch, *J. Opt. Soc. Am. B.* **10**, 283 (1993).
2. S. John, *Phys. Today* **44**, 32 (1991).
3. J. D. Joannopoulos, P. R. Villeneuve, S. Fan, *Nature* **386**, 143 (1997).
4. A. Mekis *et al.*, *Phys. Rev. Lett.* **77**, 3787 (1996).
5. V. N. Astratov *et al.*, *Nuovo Cimento D* **17D**, 1349 (1995).
6. V. Arbel-Engels *et al.*, in *Microcavities and Photonic Bandgaps*, J. Rarity and C. Weisbuch, Eds. (Kluwer Academic, Boston, 1996), pp. 125–131.
7. S. Y. Lin *et al.*, *Nature* **394**, 251 (1998).
8. J. G. Fleming and S. Y. Lin, *Opt. Lett.* **24**, 49 (1999).
9. K. M. Ho, C. T. Chan, C. M. Soukoulis, R. Biswas, M. Sigalas, *Solid State Commun.* **89**, 413 (1994).
10. N. Yamamoto and S. Noda, Proceedings of the *Tenth International Conference on Indium Phosphide and Related Materials FB2-2*, Tsukuba, Japan, 11 to 15 May 1998 (IEEE Catalog #98H36129, Piscataway, NJ, 1998).
11. N. Yamamoto, S. Noda, A. Chutinan, *Jpn. J. Appl. Phys.* **37**, L1052-4 (1998).
12. S. Noda, N. Yamamoto, H. Kobayashi, M. Okano, K. Tomoda, *Appl. Phys. Lett.* **75**, 905 (1999).
13. A. Chutinan and S. Noda, *J. Opt. Soc. Am. B* **16**, 240 (1999).
14. ———, *J. Opt. Soc. Am. B* **16**, 1398 (1999).
15. ———, *Appl. Phys. Lett.*, **75**, 3739 (1999).


20 March 2000; accepted 5 June 2000

# Synthesis and Characterization of Helical Multi-Shell Gold Nanowires

**Yukihito Kondo[1]*† and Kunio Takayanagi[1,2]**

**Suspended gold nanowires were made in an ultra-high vacuum. The finest of them was 0.6 nanometer in diameter and 6 nanometers in length. By high-resolution electron microscopy, they were shown to have a multi-shell structure composed of coaxial tubes. Each tube consists of helical atom rows coiled round the wire axis. The difference between the numbers of atom rows in outer and inner shells is seven, resulting in magic shell-closing numbers.**

Metal nanowires suspended between two electrodes have attracted much interest in recent years because the electron transport properties of a quantum wire are of importance in fundamental physics and in electronic device technology. The metal nanowires have been made with a scanning tunneling microscope (STM) and by other methods (*1–5*). The conductances in these experiments were quantized in units of $2e^2/h$, where $e$ is the electron charge and $h$ is Planck's constant (*6*, *7*). A recent experiment by simultaneous STM-TEM (transmission electron microscopy) clarified the structure and the conductance of gold nanowires (*5*). The contact in the experiment was not always a narrow neck; a wire (diameter <2 nm) was formed when the two electrodes faced each other in the [110] direction. However, the length of the wire was only 1 to 2 nm, too short for a conducting wire.

Long metal nanowires were predicted in a recent theoretical paper (*8*) to have "weird" structures that differ from the crystalline bulk. A helical structure was predicted for lead and aluminum nanowires. Carbon nanotubes also have helical structure (*9*) and are metallic or semiconducting, depending on the tube's chirality (*10–13*). Interesting physics may arise for long metal nanowires free from any supporting substrate.

Here, we report experimental evidence for multi-shell helical gold nanowires. High-resolution electron microscope images show that gold nanowires (<1.5 nm in diameter) consist of coaxial tubes. Each tube consists of helical atom rows coiled round the wire axis. The difference between the number of helical atom rows in outer and inner shells is seven, resulting in magic shell-closing numbers.

Gold nanowires were formed in an UHV (ultra-high vacuum)-TEM with the electron beam thinning technique reported previously (*14*). A gold (001) film 3 to 5 nm in thickness was cleaned by electron beam irradiation for 3 to 5 hours until the film showed the 5 × 20 reconstructed surface (*15–17*) at the specimen stage of the TEM, whose vacuum was $3 \times 10^{-8}$ Pa. The film was subsequently irradiated with a very intense electron beam (200 kV, 500 A/cm$^2$) until some holes were formed (*14*, *17*, *18*). When the bridge between two neighboring holes was narrowed, it became a long nanowire (5 to 15 nm) along the [110] direction. These nanowires (>1.5 nm in diameter) had a face-centered-cubic (fcc) structure in the core, and the lateral surfaces were reconstructed, forming a {111}-like close-packed structure (*14*). Thinned further by a weaker electron beam (10 to 50 A/cm$^2$), they exhibited new structures with widths (diameters) of 0.6 to 1.5 nm and lengths of 3 to 15 nm. The above procedure was successful only under UHV and with well-cleaned samples. We analyzed videotapes recording the thinning process of over 30 wires (a total of 10 hours of recording).

The electron microscope images in Fig. 1, A through D, show four structures that were observed during the thinning. The diameters of these wires were 1.3, 1.2, 0.9, and 0.6 nm. The dark dots in the images represent the gold atoms (or gold lattice). These dots are not arranged regularly as in the fcc lattice. The lattice fringes obliquely intersect the wire axis at an angle of 60°, whereas in a fcc lattice they would intersect at 90°. The wire images appear wavy and are asymmetrical with respect to the wire axis. Closer inspection of the images revealed that the dark dots are aligned on a line along the wire axis, which represents an atom row. In contrast to crystalline lattices, these atom rows are not straight but have wavy modulation (particularly in Fig. 1D).

During the thinning process, the wire images changed drastically when the width changed. Occasionally, the image changed even when the width remained unchanged. The duration of the steady state of the wire became shorter as the wire became thinner. We carefully selected images that showed only the steady state of the wires from the large number of frame images captured from the videotape (time interval of digitization is 1/30 s). One of the finest wires stayed for ≈0.5 s before it ruptured. We measured the distance ($d$) between the dark dots on each atom row and the width ($D$) of the wire on the selected images. As shown in Fig. 2 (upper part), $d$ was almost the nearest neighbor distance of gold (0.288 nm) for all the wires with $0.5\ \text{nm} < D < 1.5\ \text{nm}$. Although the histogram did not take the residence time (duration of the steady state) into account, the histogram for $D$ (lower part of Fig. 2) shows peaks at $D = 0.58$, 0.88, (0.96), 1.03, 1.13, 1.20, 1.29, and 1.4 nm, reflecting the stable diameters of the gold wires. We constructed structure models that explained the magic peaks in Fig. 2 and carried out TEM

[1]Takayanagi Particle Surface Project, Exploratory Research for Advanced Technology (ERATO), Akishima, Tokyo, 196-8558, Japan. [2]Tokyo Institute of Technology, Nagatuta, Midori-ku, Yokohama, Japan.

*Present address: Japan Electron Optics Laboratory (JEOL) Ltd., Akishima, Tokyo, 196-8558, Japan.
†To whom correspondence should be addressed. E-mail: kondo@jeol.co.jp

image simulations for these models by the multi-slice method (*19*, *20*).

Figure 3A shows a sheet of the triangular network composed of seven atomic rows. The sheet is rolled up to make a heptagonal tube, in which both edges (the 0th and 7th atomic rows) join at the atoms marked O and $A_1$. The direction of each atom row is oblique to the tube axis (normal to the $\mathbf{OA_1}$) by a small helical angle $H$. The helical angle $H$ is given by $\tan(H) = \mathbf{A_0A_1}/\mathbf{OA_0}$. Thus, this tube structure has helical atom rows coiled round the tube axis. The period of the helix is given by $L = nh_t/\sin(H)$, where $n$ is the number of atomic rows forming the tube ($n$ = 7 in Fig. 3A), and $h_t$ is the distance between the atomic rows (lower right panel of Fig. 3A). As the length OA determines a cross-sectional perimeter of the $n$-sided polygonal tube, a $n$-fold tube has a diameter $D_n = h_t/\{\cos(H)\ \sin(\pi/n)\}$. If we assume $d$ = 0.288 (nm), the diameter $D_n$ is approximately $0.8n$ (nm) for small helical angle $H$. The diameters at the histogram peaks in Fig. 2 were found to fit with $D_n$ values for $n$ = 7, 11, 12, 13, 14, 15, 16, and 17.5. The histogram peaks suggest that gold nanowires have a tubular structure, except for $n$ = 17.5. As illustrated in the lower right panel of Fig. 3A, the triangular lattice can deform because of the nature of the metallic bond. The value of period $L$, therefore, varies dependin; shear strain ε of the deformation (F We have carried out image simulat various values of $L$ until agreement between simulation and observation was obtained for (i) the period of the wavy image, (ii) the image asymmetry about the axis of the nanowire, and (iii) the angle between the oblique lattice fring-

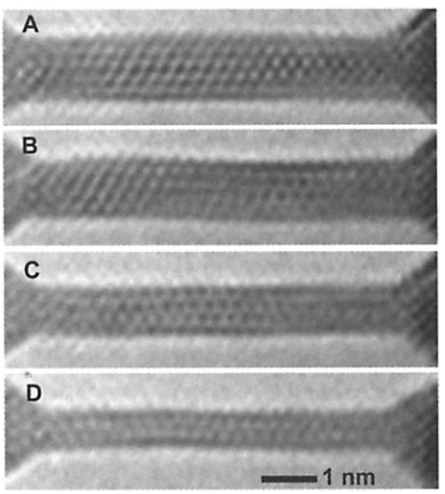


**Fig. 1.** TEM images of stable gold nanowires observed during one thinning process. The diameters of the wires in (**A**), (**B**), (**C**), and (**D**) are 1.3, 1.1, 0.8, and 0.6 nm, respectively. The dark dots represent positions of atoms projected on the image plane. The dark dots are aligned on atom rows along the wire axis. These wire images are wavy, particularly in (D).

es and wire axis. Good agreement was finally obtained for gold nanowires with a multi-shell structure consisting of coaxial tubes with $n$, $n'$, and $n''$ helical atom rows ($n > n' > n''$). The model structures are summarized in Table 1.

Here, we show how we determined a structure for the finest nanowire, which peaked at $n$ = 7 in the histogram (Fig. 2). Simulation of the seven-membered tube gave rise to a wavy and asymmetric image, similar to that in Fig. 1D. Such wavy and asymmetric images appeared only for odd-membered tubes. Even-membered tubes, even when they have helical structure, did not show the wavy image. The period of the tube $L$ was obtained from the observed image because the period of the wavy image was found to coincide with one-seventh of the period of the seven-membered helix. The seven-membered tube was found to have a single row at the center. The center row fills the cavity space of the seven-membered tube because the tube diameter is twice the nearest neighbor distance of gold ($2d$). The center atom row was found to be commensurate with the helical coils on the seven-membered tube and displaced by $d/14$ in the wire axis direction. Good agreement between the simulation and observation is seen in the upper and lower panel of Fig. 4A. This structure basically agrees with the B7 con-



thicker gold nanowires with $n$ = 11, 13, 14, and 15, although much elaborate simulation was needed. The observed TEM images were reproduced only when the outer and inner tubes had the same period. The inner and outer tubes must have the definite difference of the number of atom rows ($n - n'$ = 7), and the atoms in the inner tube must have definite relative positions with respect to the outer tube. The relative position of the inner tube in the nanowires shown on the left in Fig. 4, A through E, were obtained by minimizing the structure energies calculated with the Lennard-Jones potential. These structure models gave good agreement between the simulated and observed images

**Table 1.** Calculated diameters, measured periods, and strains of each helix in gold multi-shell nanowires. $D$, diameter; $L$, period of helix (nm); $n$, number of atom-rows in a tube; ε, lattice strain of triangle network for $d$ = 0.288 nm. Prime indicates an inner tube, and double prime indicates a central tube or row. The gold nanowires of $n$ = 12 gave only poor TEM images, and the gold nanowires of $n$ = 16 had too short a wire length (≈10 nm to estimate a period). Therefore, these models are not as conclusive as others. The $n$-$n'$-$n''$ for these wires are given in parenthesis, which were not fully tested by simulation. The polarity of ε indicates shear direction. The negative ε diminishes the helicity of a nanowire in right-handed spiral. N/A, not applicable.

| $n$-$n'$-$n''$ | $D_n$ (nm) | $D_{n'}$ (nm) | $L/d$ | ε | ε′ |
|---|---|---|---|---|---|
| 7-1 | 0.577 | N/A | 98 | −0.0357 | N/A |
| 11-4 | 0.887 | 0.353 | 288 | −0.0336 | 0.0208 |
| (12-5) | 0.965 | 0.427 | N/A | N/A | N/A |
| 13-6 | 1.043 | 0.499 | 507 | −0.0385 | 0.0177 |
| 14-7-1 | 1.122 | 0.577 | 588 | 0.036 | −0.125 |
| 15-8-1 | 1.201 | 0.652 | 865 | −0.0407 | 0.0139 |
| (16-9-2) | 1.279 | 0.731 | N/A | N/A | N/A |

(upper right and lower right panel, respectively, in Fig. 4, B through E).

The inner and outer shells always have even-odd or odd-even coupling, and $n - n'$ is seven (a single atom chain is regarded as ıbered in this discussion). The differ- ween $D_n$ and $D_n'$ is approximately $2d$ ). The difference between the perimeters of the inner and outer tubes is $2\pi d$. The outer tube should have more space for seven atom rows than the inner tube because the ratio of the perimeter difference to the distance between atom rows ($h_t$) is 7.25. This consideration explains the rule that $n - n'$ = 7. We also noticed the following. Each of gold nanowires from $n$ = 7 to 13 has a double-walled shell, and those from $n$ = 14 to 16 have a triple-walled shell. Nanowires with $n$ = 1 to 6 are supposed to have a single-walled shell. Thus, a new wall arises at every increase of seven atom rows to close the shell. This shell-closing rule explains the multi-shell structures of gold nanowires that have the magic shell-closing numbers.

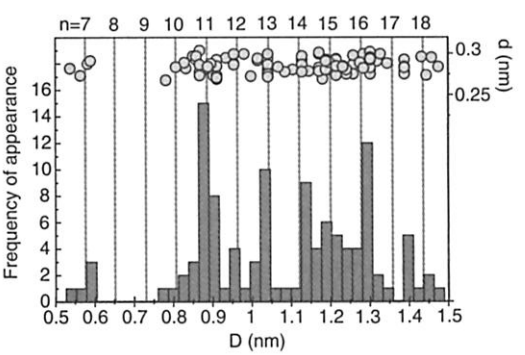


**Fig. 2.** Dot-to-dot distance ($d$) in each atom row (upper) and histogram for the appearance of gold nanowires with diameter ($D$) (lower). For over 30 wires in thinning processes (length >5 nm; width < 2 nm), $d$ and $D$ were measured. Length scale calibration was done with the lattice images of the gold film around the gold nanowire. Vertical gray lines indicate the diameters of the $n$-membered tubes, given by $D_n = h_t/\cos(H)\ \sin(\pi/n)$, where $h_t = \sqrt{3}(d/2)$ and $d$ = 0.288 nm (Fig. 3A). $D_n$ is insensitive to the helical angle $H$ (Fig. 3A). The diameters at histogram peaks coincide with the calculated $D_n$.

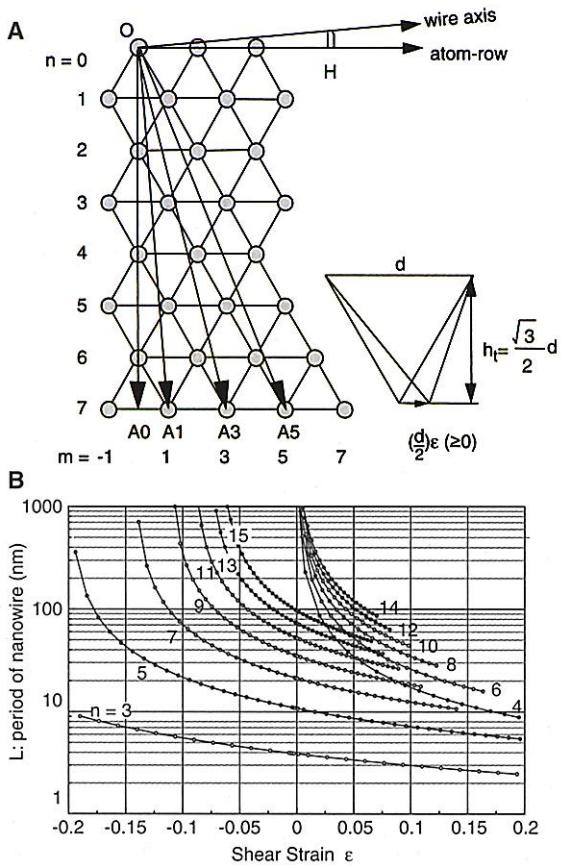


**Fig. 3 (left).** (**A**) Triangular network sheet of a seven-membered tube. Each triangle has the $d$ and the $h_t$ and is deformed by $\varepsilon$, as shown in the schematic diagram (lower right), where $d$ is interatomic distance, $h_t$ is distance between neighboring atom rows, and $m$ is the chiral order for the helix. $\mathbf{OA}_m$ is given generally as $[h_t n, (m + n\varepsilon)(d/2)]$; in this figure, $n = 7$ and $m = 1$. The helical angle $H$, given by $\tan(H) = (m/n + \varepsilon)\, d/2h_t$, defines the angle between the atom row and the wire axis. Positive $H$ makes a right-handed spiral of the atom row. The helical angle determines the period ($L$) and diameter ($D$) of the tube, as $L \sin(H) = nh_t$, and $D \sin(\pi/n) = h_t/\cos(H)$, respectively. (**B**) Period of the helix ($L$) calculated for the odd-membered tubes ($n$ = 7, 9, 11, and 15 for $m$ = 1) and for the even-membered tubes ($n$ = 4, 6, and 8 for $m = 0$) with the values listed in caption of Fig. 3.

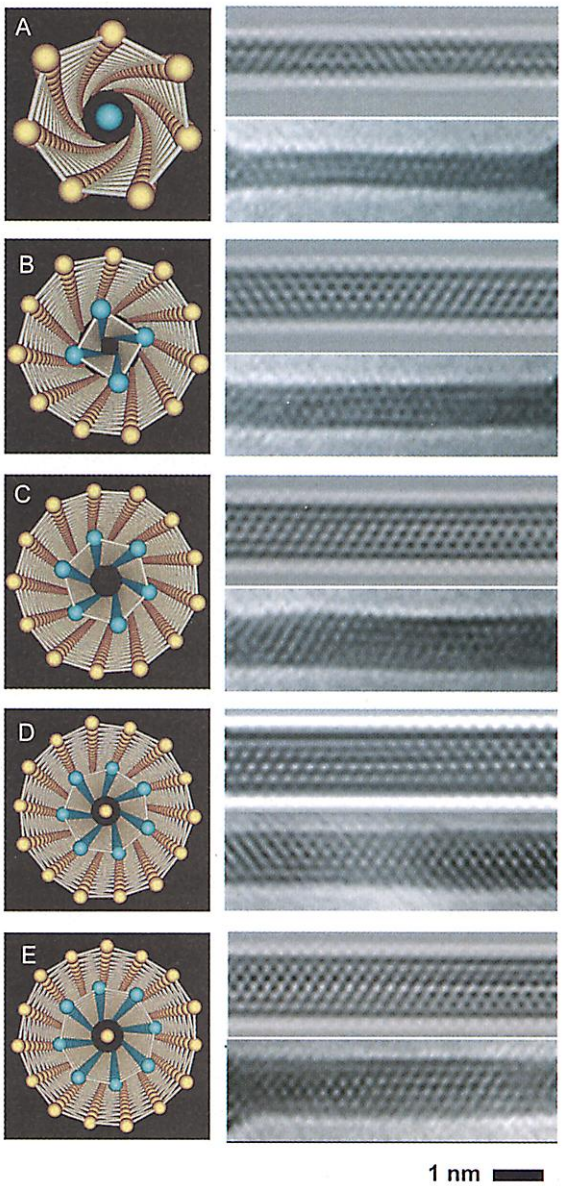


**Fig. 4 (right).** Models, simulated, and observed images of multi-shell structures of the gold nanowires. Models in right panels (**A** through **E**) are axial view of the 7-1, 11-4, 13-6, 14-7-1, and 15-8-1 structures. The $n$-fold helix of each shell is composed of a tube with a triangular network. Corresponding simulated images (upper) and observed images (lower) for the gold nanowires are in the right panels. Image in (D) for the even-membered outer shell gives no wavy asymmetric appearance. The imaging conditions used in simulation and experiment are as follows. Spherical and chromatic aberration coefficients of the objective lens were 0.7 mm and 1.2 mm, respectively. Incident electron beam energy was 200 keV. Energy spread of the primary beam was 1.0 eV. Illumination angle of the beam was 0.5 mrad. The focus was +55 nm. For the multi-slice simulation, the model structure with unit cell (7.2 nm × 2.88 nm × 1.5 nm) was sliced into five thin layers, and 256 × 256 diffracted waves were used.

As seen in the histogram in Fig. 2, peak height of odd-membered tubes decreases in the order of $n$ = 11, 13, 15, and 17. In contrast, that of even-membered tubes increases in the order of $n$ = 12, 14, and 16. Because the inner and outer shells have odd-even or even-odd coupling, the inner tube is even-membered for the odd-membered outer tube and odd for the even one. Knowing that the inner and outer tubes have the same period, the strain ε for the odd-membered inner tube becomes large as the tube's diameter decreases to match the tube's period with that of the even-membered outer tube (Fig. 3B). Therefore, for the even-odd coupling ($n - n'$), the stability of the inner tube decreases as the diameter decreases. In contrast, for the odd-even coupling, the strain ε on the inner tube caused by matching the periods of the inner and outer tubes is not so large because the periods of the tubes naturally increase as their diameters increase ($n > n'$). Therefore, the nanowires with odd-membered outer tubes are more stable than those with even-membered outer tubes for small diameters ($n$ = 7, 11, 13).

One exceptional histogram peak is the one at $n$ = 17.5. We believe the wire at this peak to have an intermediate structure between the multi-shell and the hexagonal prism structure because the thick wires have the hexagonal prism structure (*14*).

Although we report the existence of helical tubes only in gold, such magic multi-shell structures might also be found in other metal nanowires. Quantum transport of the conduction electrons in these structures may be important in connection with applications in quantum devices.

**References**

1. N. Agrait, N. J. Rodrigo, S. Vieria, *Phys. Rev. B* **47**, 12345 (1993).
2. J. I. Pascual *et al.*, *Science* **267**, 1793 (1995).
3. L. Olesen *et al.*, *Phys. Rev. Lett.* **72**, 2251 (1994).
4. J. I. Costa-Kramer *et al.*, *Phys. Rev. B* **55**, 1022 (1997).
5. H. Ohnishi, Y. Kondo, K. Takayanagi, *Nature* **395**, 780 (1998).
6. L. Landauer, *IBM J. Res. Dev.* **1**, 223 (1957).
7. B. J. van Wees *et al.*, *Phys. Rev. Lett.* **60**, 848 (1988).
8. O. Gulseren, F. Ercolessi, E. Tosatti, *Phys. Rev. Lett.* **80**, 3775 (1998).
9. S. Iijima, *Nature* **354**, 56 (1991).
10. J. W. G. Wildöer *et al.*, *Nature*, **391**, 59 (1998).
11. J. W. Mintmire, B. L. Dunlap, C. T. White, *Phys. Rev. Lett.* **68**, 631 (1992).
12. A. Thess *et al.*, *Science* **273**, 483 (1996).
13. T. W. Ebbesen *et al.*, *Nature* **382**, 54 (1996).
14. Y. Kondo and K. Takayanagi, *Phys. Rev. Lett.* **79**, 3455 (1997).
15. M. A. Van Hove *et al.*, *Surf. Sci.* **103**, 189 (1981).
16. K. Yamazaki, K. Takayanagi, Y. Tanishiro, K. Yagi, *Surf. Sci.* **199**, 595 (1988).
17. K. Niwase, W. Siegle, A. Phillipp, A. Seeger, *Philos. Mag.* **74**, 167 (1996).
18. D. Cherns, *Surf. Sci.* **90**, 339 (1979).
19. J. M. Cowley and A. F. Moodie, *Acta Crystallogr.* **10**, 609 (1957).
20. J. Urban, H. Sack-Kongehl, K. Weiss, *Z. Phys. D* **28**, 247 (1993).

22 March 2000; accepted 14 June 2000